

A Method for Estimating Wind-Driven Frictional, Time-Dependent, Stratified Shelf and Slope Water Flow

ALLAN J. CLARKE AND STEPHEN VAN GORDER

Department of Oceanography, The Florida State University, Tallahassee, FL 32306

(Manuscript received 3 December 1984, in final form 31 October 1985)

ABSTRACT

Friction, the alongshore pressure gradient and time-dependent effects are all of lowest-order importance in the dynamics of wind-driven fluctuating currents and sea levels on continental shelves. Previous work has shown that when all these effects are included, the ocean response can be described by an infinite sum of coastal-trapped waves whose amplitudes satisfy a fully coupled infinite set of forced, first-order wave equations. We present a practical method for solving this coupled set of equations for general low-frequency, large-scale wind stress forcing as input. Convergence properties of the solution are examined analytically. For the same accuracy, more modes are required to describe alongshore currents than sea level and fewer modes are required to describe barotropic than depth-dependent motion.

As an example, numerical calculations were carried out for a model of the West Florida Shelf. The sea level field was effectively described by one mode but the alongshore velocity field was not. Seven modes were necessary to represent the solution accurately. Decoupling the equations by setting off diagonal elements of the friction coupling coefficients equal to zero significantly changed the alongshore velocity amplitude. For realistic parameter values the Gill and Schumann frictionless alongshore velocity field and the Arrested-Topographic Wave alongshore velocity field differed significantly from that of the more general case.

1. Introduction

Scale analysis of the equations of motion applied to wind-driven fluctuations at "weather" frequencies ($2\pi/\text{few days}$ to $2\pi/\text{few weeks}$) on a continental shelf shows that friction, the alongshore pressure gradient and time-dependent effects are *all* of lowest-order importance to the dynamics. Early theories of wind-driven fluctuations on shelves either included the alongshore pressure gradient and time dependence but added dissipational effects in an ad hoc manner (Gill and Schumann, 1974; Gill and Clarke, 1974; Clarke, 1977) or neglected time-dependent effects (Csanady, 1978). Brink and Allen (1978) and Brink (1982) showed that when all three effects are included the forced coastal trapped wave equations describing the inviscid shelf-water response become coupled together. Brink and Allen (1978) and Brink (1982) then used these equations to obtain results for small friction and idealized wind forcing. We intend to provide a practical method for solving the infinite set of fully coupled equations for measured wind forcing and realistic friction.

The next section establishes the infinite set of coupled equations from first principles. While the infinite coupled set has the same form as that described by Brink (1982), expressions for the coupling coefficients differ. A method of solution for the coupled problem is then described and discussed in section 3. Convergence properties are considered in section 4 and then a West

Florida Shelf example is considered in section 5. Concluding remarks are presented in section 6.

2. Theory

a. Equations and boundary conditions

Following Clarke and Brink (1985), the field equation and boundary conditions for linear, large-scale, low-frequency wind-driven flow over a continental margin can be written in terms of p , the pressure perturbation due to the motion, as

$$p_{xxt} + f^2 \left(\frac{p_{zt}}{N^2} \right)_z = 0, \quad (2.1)$$

$$p_{xt} + \frac{rp_x}{h} + fp_y = \frac{f\tau^y}{h} \quad \text{at } x = b, \quad (2.2a)$$

$$p_z = 0 \quad \text{at } z = 0, \quad (2.2b)$$

$$\frac{f^2 p_{zt}}{N^2} + h_x(p_{xt} + fp_y) + (rp_x)_x - h_x rp_{xz} = 0 \quad \text{at } z = -h, \quad (2.2c)$$

$$p_x \rightarrow 0 \quad \text{as } x \rightarrow \infty. \quad (2.2d)$$

In these equations x , y , z , t , N , f and τ^y refer, respectively, to distance seaward of and perpendicular to the straight coast at $x = 0$, distance alongshore, distance vertically upward from the ocean surface, time,

the buoyancy frequency, the Coriolis parameter and the alongshore component of the wind stress. The water depth $h(x)$ increases monotonically until the constant-depth sea region begins. The parameter r is the usual friction coefficient and is defined from the equation

$$\tau_B^y = \rho_0 r v_B \tag{2.3}$$

where τ_B^y is the y component of the bottom stress, ρ_0 is the mean water density and v_B is the alongshore component of velocity at the bottom. In (2.2a), $x = b$ corresponds to a depth equal to three times the Ekman layer e -folding decay scale δ . Equation (2.2a) is equivalent to the condition that the depth integrated velocity perpendicular to the shore vanishes at $x = b$ (Mitchum and Clarke, 1986a).

b. Analysis

Let

$$\mathbf{M} = \left(\frac{p_x}{f^2}\right)\mathbf{i} + \left(\frac{p_z}{N^2}\right)\mathbf{k} \tag{2.4}$$

$$\nabla = \mathbf{i} \frac{\partial}{\partial x} + \mathbf{k} \frac{\partial}{\partial z} \tag{2.5}$$

where \mathbf{i} and \mathbf{k} are unit vectors in the direction of increasing x and z respectively. In terms of \mathbf{M} , the field equation and boundary conditions can be written

$$\nabla \cdot \mathbf{M}_t = 0, \tag{2.6}$$

$$\mathbf{n} \cdot \mathbf{M}_t = 0 \quad \text{on } z = 0, \tag{2.7a}$$

$$\mathbf{n} \cdot \mathbf{M}_t = \frac{p_y}{f} + \frac{rp_x}{f^2 h} - \frac{\tau^y}{fh} \quad \text{at } x = b, \tag{2.7b}$$

$$\mathbf{n} \cdot \mathbf{M}_t = [1 + (h_x)^2]^{-1/2} \left[\frac{h_x p_y}{f} + \frac{(rp_x)_x}{f^2} - \frac{h_x rp_{xz}}{f^2} \right] \tag{2.7c}$$

at $z = -h(x)$

$$p_x \rightarrow 0 \quad \text{as } x \rightarrow \infty \tag{2.7d}$$

where \mathbf{n} is the unit outward vector to the boundary Γ defined by $x = b$, $z = 0$, $x = \infty$ and $z = -h(x)$.

The frictionless free-wave coastal trapped eigenfunction problem corresponding to (2.6) and (2.7) is (Clarke, 1977):

$$\nabla \cdot \mathbf{B} = 0, \tag{2.8}$$

$$\mathbf{n} \cdot \mathbf{B} = 0 \quad \text{on } z = 0, \tag{2.9a}$$

$$(\mathbf{n} \cdot \mathbf{B})c = \frac{F}{f} \quad \text{on } x = b, \tag{2.9b}$$

$$(\mathbf{n} \cdot \mathbf{B})c = h_x [1 + (h_x)^2]^{-1/2} \frac{F}{f} \quad \text{on } z = -h, \tag{2.9c}$$

$$F_x \rightarrow 0 \quad \text{as } x \rightarrow \infty \tag{2.9d}$$

where

$$\mathbf{B} = \frac{F_x}{f^2} \mathbf{i} + \frac{F_z}{N^2} \mathbf{k} \tag{2.9e}$$

and F and c are the eigenfunction and eigenvalue of the problem.

From (2.6) and (2.8) we have the identity

$$\nabla \cdot \left(F_j \frac{\partial \mathbf{M}}{\partial t} - p_t \mathbf{B}_j \right) = 0$$

where the subscript j refers to the j th mode. By the divergence theorem, this equation can be written

$$\oint_{\Gamma} \mathbf{n} \cdot \left(F_j \frac{\partial \mathbf{M}}{\partial t} - p_t \mathbf{B}_j \right) ds = 0. \tag{2.10}$$

Use of the boundary conditions (2.7) and (2.9) in (2.10) then results in

$$\int_{x=b} F_j \left[p_y + \frac{rp_x}{(hf)} - \frac{\tau^y}{h} - \frac{p_t}{c_j} \right] ds + \int_{z=-h} F_j \left(h_x p_y + \frac{(rp_x)_x}{f} - \frac{h_x rp_{xz}}{f} - \frac{h_x p_t}{c_j} \right) \times [1 + (h_x)^2]^{-1/2} ds = 0 \tag{2.11}$$

or, more explicitly,

$$\int_{-h(b)}^0 \left[F_j \left(p_y - \frac{p_t}{c_j} \right) \right]_{x=b} dz + \int_{-h(b)}^0 \left[\frac{F_j r p_x f^{-1}}{h} \right]_{x=b} dz + \int_b^\infty \left[F_j \left(p_y - \frac{p_t}{c_j} \right) \right]_{z=-h(x)} h_x dx + \int_b^\infty F_j(x, -h) \frac{d}{dx} \{ r p_x [x, -h(x)] \} / f dx = \left(\int_{-h(b)}^0 F_j(b, z) dz \right) \frac{\tau^y(y, t)}{h(b)}. \tag{2.12}$$

Since the eigenfunctions $F_i(x, z)$ form a complete set of functions, we may write

$$p = \sum_{i=1}^\infty F_i(x, z) \phi_i(y, t). \tag{2.13}$$

Substitution of this expression for p into (2.12) and use of the orthogonality property of the eigenfunctions (Clarke, 1977) implies that the ϕ_j must satisfy

$$-\frac{1}{c_j} \frac{\partial \phi_j}{\partial t} + \frac{\partial \phi_j}{\partial y} + \sum_{i=1}^\infty a_{ij} \phi_i = b_j \tau^y(y, t) \tag{2.14}$$

where

$$b_j = \frac{1}{h(b)} \int_{-h(b)}^0 F_j(b, z) dz / D_j, \tag{2.15}$$

$$a_{ij} = D_j^{-1} \left[\int_b^\infty F_j(x, -h) \frac{d}{dx} [r F_{ix}(x, -h)] f^{-1} dx + \int_{-h(b)}^0 [F_j r F_{ix} f^{-1} h^{-1}]_{x=b} dz \right] \tag{2.16}$$

and

$$D_j = \int_{-h(b)}^0 [(F_j)^2]_{x=b} dz + \int_b^\infty [(F_j)^2]_{z=-h(x)} h_x dx. \quad (2.17)$$

The eigenfunctions are determined up to an arbitrary multiplicative constant and it is customary to normalize F_j so that $D_j = 1$. Because $h_x dx = dh$, (2.17) then implies that F_j has the dimension (depth)^{-1/2}. We prefer to make F_j dimensionless and choose the arbitrary constant so that $F_j(b, 0) = 1$. Then D_j has the dimensions of depth and the "amplitude" ϕ_j in (2.13) has the same dimension as p .

Note that in obtaining (2.14) it appears at first sight that we used

$$\begin{aligned} & \frac{d}{dx} \left\{ r \left[\frac{\partial}{\partial x} \left(\sum_{i=1}^\infty F_i(x, z) \phi_i(y, t) \right) \right]_{z=-h(x)} \right\} \\ &= \sum_{i=1}^\infty \phi_i(y, t) \frac{d}{dx} \left[r \frac{\partial F_i}{\partial x} [x, -h(x)] \right]. \end{aligned} \quad (2.18)$$

Such an exchange of differentiation and infinite summation is only possible if the resultant infinite series on the right-hand side of (2.18) is uniformly convergent. We will see later that this is not always the case. Consequently, we point out that (2.14) can be obtained under the milder assumption

$$\frac{\partial}{\partial x} \left[\sum_{i=1}^\infty F_i \phi_i \right] = \sum_{i=1}^\infty F_{ix} \phi_i. \quad (2.19)$$

To see this, observe that the last integral on the left-hand side of (2.12) can be integrated by parts to give

$$\begin{aligned} & \int_b^\infty F_j(x, -h) \frac{d}{dx} \{ r p_x [x, -h(x)] \} / f dx \\ &= [-r p_x F_j / f]_{x=b}^{z=-h} - \int_b^\infty f^{-1} [r p_x]_{z=-h} \\ & \quad \times \frac{d}{dx} \{ F_j [x, -h(x)] \} dx \end{aligned} \quad (2.20)$$

so that we need only (2.19) to proceed to (2.14). The a_{ij} obtained by this approach are the same as (2.16) as can be seen by reversing the integration-by-parts process with F_i now replacing p .

Clarke (1977) obtained (2.14) in the frictionless case (a_{ij} all zero). Brink (1982) obtained (2.14) by a slightly different approach and different coefficients a_{ij} resulted. In the limit that the bottom boundary layer thickness is negligible compared to interior vertical scales, Brink's expression for a_{ij} is effectively (2.16) with, in our notation, an extra term

$$-D_j^{-1} \int_b^\infty r f^{-1} [F_{ix} F_{jz}]_{z=-h(x)} h_x dx$$

on the right-hand side. This term vanishes in the barotropic case but not in the baroclinic.¹ The discrepancy in the a_{ij} result appears to arise because in Brink's vorticity equation (see Eq. 2.10a of his paper) the Ekman layer is apparently over-prescribed and the pressure field is consequently forced to adjust over the boundary layer scale. In our formulation, based on Clarke and Brink (1985), boundary layer dynamics are automatically taken into account in the boundary conditions.

3. Method of solution

Once the solution (2.13) has been obtained, it is possible to estimate commonly measured quantities, e.g., alongshore velocity

$$v = \frac{p_x}{f} = \sum_{i=1}^\infty F_{ix} f^{-1} \phi_i. \quad (3.1)$$

Therefore, in order to obtain estimates of measurable quantities, all we need to do is to obtain the inviscid eigenfunctions F_i and the amplitude functions ϕ_i . The F_i can be obtained by resonance iteration (Wang and Mooers, 1976; Brink, 1982) and the ϕ_i can be obtained by using the technique described as follows.

a. Calculation of the ϕ_i

By (2.14), we need to solve the equation

$$-\frac{1}{c_j} \phi_{jt} + \phi_{jy} + a_{ij} \phi_j = b_j \tau^y(y, t) - \sum_{\substack{i=1 \\ i \neq j}}^\infty a_{ij} \phi_i. \quad (3.2)$$

Since long coastal trapped waves travel in only one direction along a coastline for monotonic $h(x)$ (Clarke, 1977), (3.2) must be subject to a boundary condition at some starting position $y = 0$. Mathematically,

$$\phi_j(0, t) = \text{known function}. \quad (3.3)$$

Note that by our choice of axes, the waves travel in the negative y -direction in the Northern Hemisphere and the positive y -direction in the Southern Hemisphere. This means that in what follows, $c_j > 0$, $\Delta y < 0$ and $a_{ij} < 0$ in the Northern Hemisphere and $c_j < 0$, $\Delta y > 0$ and $a_{ij} > 0$ in the Southern Hemisphere.

The problem defined by (3.2) subject to (3.3) is solved by characteristics. Along the characteristic $t = t_j(y)$ defined by

$$\frac{dt_j}{dy} = -\frac{1}{c_j(y)}, \quad (3.4)$$

¹ Numerical differences are negligible for near-barotropic conditions $S \leq 0.1$ (Brink's notation). For larger S , Brink's values of a_{11} can be different by as much as 26% in reasonable examples. For higher modes, the discrepancy can be greater (100%). Brink's conclusion that increased stratification decreases wave damping remains true.

(3.2) can be written

$$\frac{d\phi_j}{dy} + a_{ij}(y)\phi_j = G_j(y, t_j(y)) \quad (3.5)$$

where

$$G_j(y, t_j(y)) = b_j(y)\tau^y(y, t) - \sum_{\substack{i=1 \\ i \neq j}}^M a_{ij}(y)\phi_i(y, t). \quad (3.6)$$

In (3.2) observe that c_j , a_{ij} and b_j have been taken to be functions of y . This y -variation is induced by allowing variations in bottom topography and N^2 alongshore in the same way as done by Gill and Schumann (1974) and Gill and Clarke (1974). Note also that in (3.6) the sum in the last term is finite instead of infinite. A guide to how large M has to be will be given by convergence criteria discussed in the next section.

Equation (3.5) may also be written

$$\frac{d}{dy} \{ \phi_j[y, t_j(y)]E(y) \} = G_j(y, t_j(y))E(y) \quad (3.7)$$

where $E(y)$ is the integrating factor

$$E(y) = \exp \left[\int_0^y a_{ij}(y') dy' \right]. \quad (3.8)$$

Integration of (3.7) from $y - \Delta y$ to y gives

$$\begin{aligned} \phi_j(y, t_j(y)) &= \phi_j[y - \Delta y, t_j(y - \Delta y)]E(y - \Delta y)/E(y) \\ &+ \int_{y - \Delta y}^y G_j(y_*, t_j(y_*))E(y_*)/E(y) dy_*. \end{aligned} \quad (3.9)$$

In (3.9), by (3.4) and the boundary condition $t_j(y) = t$

$$t_j(y^*) = t + \int_y^{y^*} \frac{dy_*}{c_j(y_*)}. \quad (3.10)$$

For small Δy (3.9) and (3.10) can be reduced, by the trapezoidal rule of integration to

$$\begin{aligned} \phi_j(y, t) &= \phi_j[y - \Delta y, t_j(y - \Delta y)] \\ &\times \exp \left[-\frac{\Delta y}{2} [a_{ij}(y) + a_{ij}(y - \Delta y)] \right] \\ &+ \left\{ G_j(y, t) + G_j[y - \Delta y, t_j(y - \Delta y)] \right\} \\ &\times \exp \left[-\frac{\Delta y}{2} [a_{ij}(y) + a_{ij}(y - \Delta y)] \right] \frac{\Delta y}{2} \end{aligned} \quad (3.11)$$

where

$$t_j(y - \Delta y) = t + \frac{\Delta y}{2} \left[\frac{1}{c_j(y)} + \frac{1}{c_j(y - \Delta y)} \right]. \quad (3.12)$$

Using (3.6) enables (3.11) to be written as the matrix equation

$$\phi \left(\mathbf{I} + \mathbf{K} \frac{\Delta y}{2} \right) = \mathbf{q}. \quad (3.13)$$

In (3.13) ϕ is a row vector with elements $\phi_j(y, t)$, \mathbf{I} is the $M \times M$ identity matrix, \mathbf{q} is the row vector with elements q_j given by

$$\begin{aligned} q_j &= b_j(y)\tau^y(y, t) \frac{\Delta y}{2} + \phi_j[y - \Delta y, t_j(y - \Delta y)] \\ &\times \exp \left[-\frac{\Delta y}{2} [a_{ij}(y) + a_{ij}(y - \Delta y)] \right] \\ &+ \left\{ G_j[y - \Delta y, t_j(y - \Delta y)] \right. \\ &\left. \times \exp \left[-\frac{\Delta y}{2} [a_{ij}(y) + a_{ij}(y - \Delta y)] \right] \right\} \frac{\Delta y}{2} \end{aligned} \quad (3.14)$$

and \mathbf{K} is the matrix with elements

$$k_{ij} = \begin{cases} 0, & i = j \\ a_{ij}, & i \neq j. \end{cases} \quad (3.15)$$

The integration interval Δy is to be very small compared to the dissipation scales $(a_{ij})^{-1}$ and so $\mathbf{K}\Delta y/2$ is a matrix with elements that are very small compared with one. Hence, within a small error $\mathbf{K}^2(\Delta y)^2/4$,

$$\left[\mathbf{I} + \mathbf{K} \frac{\Delta y}{2} \right]^{-1} = \left(\mathbf{I} - \mathbf{K} \frac{\Delta y}{2} \right) \quad (3.16)$$

and consequently

$$\phi = \mathbf{q} \left(\mathbf{I} - \mathbf{K} \frac{\Delta y}{2} \right). \quad (3.17)$$

Equation (3.17) indicates that if $\phi_j[y - \Delta y, t_j(y - \Delta y)]$ is known then $\phi_j(y, t)$ may be calculated. Since ϕ_j is known at $y = 0$, we can therefore calculate ϕ at $y = \Delta y$, then use the ϕ results at $y = \Delta y$ in \mathbf{q} to calculate ϕ at $y = 2\Delta y$, etc. In this manner, ϕ can be found at all grid points on the y -axis.

b. Practical application of the method for finding ϕ_i

1) THE WIND STRESS FIELD

The wind stress field $\tau^y(y, t)$ is approximated by a number of locations along the real coast using linear interpolation.

2) THE BOUNDARY CONDITION AT $y = 0$

For the integration to be carried out, ϕ must be known at $y = 0$. There are at least three possible ways to take this boundary condition into account.

(i) Far enough away from the location $y = y_0$ of interest, $\phi(0, t)$ may be taken to be zero (Gill and Clarke, 1974; Gill and Schumann, 1974; Clarke, 1977; Battisti and Hickey, 1984). Such an approximation is reasonable if either

1) no significant forcing occurs in the region from where the free waves would have propagated to $y = 0$ ($y > 0$ in Fig. 1); or

2) $|y_0|$ is significantly greater than the damping scale for the least damped coastally trapped wave mode ($|a_{jj}y_0|$ large enough for all j).

(ii) If adequate measurements are available at the given coastal section $y = 0$, ϕ can be found by a least-squares fit of (say) the alongshore current measurements to

$$v = f^{-1} \sum_j F_{jx} \phi_j$$

so that the $\phi_j(0, t)$ are determined. This procedure was used in the Australian Coastal Experiment (Church et al., 1986).

(iii) If only coastal sea level is known at $y = 0$ and one chooses not to use (i), then since the coastal adjusted sea level η is usually dominated by the first mode we can write

$$\begin{aligned} \eta(b, 0, t) &= \rho_0^{-1} g^{-1} p(b, 0, 0, t) \\ &\approx \rho_0^{-1} g^{-1} F_1(b, 0) \phi_1(0, t) \end{aligned} \quad (3.18)$$

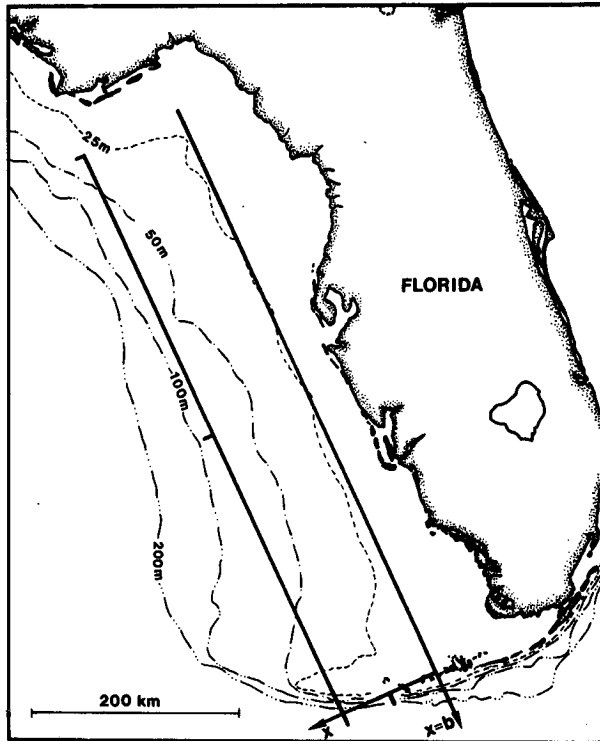


FIG. 1. The West Florida Shelf and the borders of the model. The y axis points roughly southeastward and parallel to $x = b$. The tick marks on the southern border correspond to $b + 50$ km and $b + 100$ km; those on the western border to $y = -300$ km and $y = -600$ km. Model water depth increases linearly from 22.5 m at $x = b$ to 80 m at $x = b + 100$ km. The southern end of the model is closed because no energy enters through this end. Energy leaves unhindered through the northern end.

where ρ_0 is the mean water density. Thus ϕ at $y = 0$ is estimated as

$$\begin{aligned} \phi_j(0, t) &= \rho_0 g \eta(b, 0, t) \quad \text{for } j = 1 \\ &= 0 \quad \text{for } j \neq 1 \end{aligned} \quad (3.19)$$

where we have used $F_1(b, 0) = 1$. Note that although mode one may dominate the coastal pressure, several modes may contribute to alongshore velocity and (3.19) would thus introduce a possibly significant error by assuming $\phi_j = 0$ for $j \geq 2$. However, in some cases the higher-mode energy flux entering $y = 0$ is small enough that the approximation (3.19) does not introduce serious error (Mitchum and Clarke, 1986b).

3) RESTRICTIONS ON Δy AND THE TIME INTERVAL OF INTEGRATION Δt

Another necessary detail in applying the method is that there are some restrictions on Δy and the wind-stress time series interval Δt . One restriction is that we must integrate slowly enough so that we resolve the slowest propagating wave, i.e.,

$$\frac{\Delta y}{\Delta t} \leq \min_j c_j = c_M. \quad (3.20)$$

A second restriction is that the trapezoidal rule must do an adequate job in approximating the integral in (3.9). An estimate of the relative error in using the trapezoidal rule is

$$\begin{aligned} &\left(\text{maximum}_{y-\Delta y \leq y_* \leq y} \frac{d^2}{dy_*^2} [G_j(y_*, t_j(y_*)) E(y_*)] \right) \frac{(\Delta y)^3}{12} / \\ &\int_{y-\Delta y}^y G_j(y_*, t_j(y_*)) [E(y_*)] dy_* \approx \frac{(a_{jj})^2 (\Delta y)^2}{12}. \end{aligned}$$

Since a_{jj} increases with increasing j (see section 4), Δy must be chosen small enough so that

$$\frac{(a_{MM})^2 (\Delta y)^2}{12} \ll 1. \quad (3.21)$$

A final restriction is that the error in getting (3.17) must be small, i.e.,

$$\max_{i,j} \left| \sum_{m=1}^M k_{im} k_{mj} \right| \frac{(\Delta y)^2}{4} \ll 1. \quad (3.22)$$

In the West Florida Shelf example given in section 5, conditions (3.20)–(3.22) could all be met with $\Delta t = 10.9$ h and $\Delta y = 600$ m.

4) SPINUP TIME

Since any practical wind-stress time series is of finite length, in applying the model it is necessary that the wind-stress forcing be suddenly started at a certain time. It is useful, therefore, to know the “spinup” time, i.e., the time it takes the model to “forget” that the wind

stress started abruptly. In the frictionless case this adjustment time is the time taken for the slowest mode (mode M) to travel from $y = 0$ to the observing section $y = y_0$. When friction is present, however, higher modes are usually damped strongly enough that signals leaving $y = 0$ never reach $y = y_0$. In this case we would expect the spinup time to be the maximum time taken (over all modes j) for mode j to travel its damping scale distance $|a_{jj}|^{-1}$, i.e., a time $\max\{(-c_j a_{jj})^{-1}\}$. This may be seen mathematically from (3.2) and (3.6). Since c_j^{-1} and a_{jj} increase like j or j^2 for large j (see section 4), (3.2) can be simplified to

$$\frac{\partial \phi_j}{\partial t} - c_j a_{jj} \phi_j = -c_j G_j(y, t). \quad (3.23)$$

This equation can be integrated from some starting time t_1 to a general time t to get

$$\begin{aligned} \phi_j(y, t) = & \phi_j(y, t_1) \exp[-c_j a_{jj}(t_1 - t)] \\ & - c_j \int_{t_1}^t G_j(y, t_*) \exp[-c_j a_{jj}(t_* - t)] dt_*. \end{aligned} \quad (3.24)$$

Since $-c_j a_{jj} > 0$, mode j does not "remember" the initial condition at time t_1 provided $t - t_1$ is several times the mode j e -folding spin-up time, $(-c_j a_{jj})^{-1}$. This implies that model predictions will only be accurate several times

$$\max_j \{(-c_j a_{jj})^{-1}\}$$

after the start of the wind-forcing. Estimation of the spin-up time in the limiting barotropic and purely baroclinic cases will be discussed in section 4.

4. Convergence properties

To investigate convergence properties of the solution, we will examine solutions for the limiting cases of barotropic flow and purely baroclinic flow and then discuss the more general case.

a. Convergence properties in the barotropic case

Clarke and Brink (1985) have shown that at weatherband frequencies ($2\pi/\text{few days}$ to $2\pi/\text{few weeks}$), wind-driven motions on continental shelves are barotropic, confined to the shelf and satisfy a condition of zero pressure at the shelf edge if

$$\left| \frac{N_s \alpha_s}{f} \right| \ll 1. \quad (4.1)$$

In (4.1) N_s and α_s refer to shelf-averaged buoyancy frequency and shelf-averaged bottom slope respectively. Thus in the limit described by (4.1), the long coastal-trapped wave eigenfunctions are independent of z and satisfy the Sturm-Liouville problem

$$F_{xx} + \frac{h_x F_x}{h} + \frac{\mu h_x F}{h} = 0, \quad (4.2)$$

$$F_x + \mu F = 0 \quad \text{at } x = b, \quad (4.3a)$$

$$F = 0 \quad \text{at } x = a, \quad (4.3b)$$

where $x = a$ denotes the edge of the shelf and

$$\mu = \frac{f}{c}. \quad (4.3c)$$

To analyze solution properties in the barotropic case, we need to know the properties of the eigenfunctions $F_j(x)$ and eigenvalues c_j for large mode number j . A WKB analysis in appendix A shows that

$$\begin{aligned} F_j(x) = & (h_x h)^{-1/4} [(h_x h)^{1/4}]_{x=b} \sin\{(j-1)\pi T T_b^{-1}\} \\ & \times \{1 + O[(j-1)^{-1}]\} \end{aligned} \quad (4.4a)$$

$$c_j = \frac{f T_b^2}{(j-1)^2 \pi^2} \{1 + O[(j-1)^{-2}]\} \quad (4.4b)$$

where

$$T(x) = - \int_a^x \left(\frac{h_x}{h} \right)^{1/2} dx \quad (4.5a)$$

$$T_b = T(b). \quad (4.5b)$$

Note that asymptotically $F_j(b) = 0$ and so we cannot choose $F_j(b) = 1$ in this particular case. However, in the same spirit as the discussion following (2.17), $F_j(x)$ in (4.4a) is dimensionless and $O(1)$. The properties of the coefficients in the barotropic case are derived in appendix A and are displayed in Table 1.

Note that the barotropic case is surprising because the phase speed $c_j \sim j^{-2}$ rather than the j^{-1} dependence expected in the general case (Clarke, 1977). This apparent contradiction can be resolved by noting that for large mode number j , the barotropic approximation breaks down. This can be seen from the perturbation analysis of Clarke (1976) which shows that coastal-trapped wave eigenfunctions must satisfy

$$1 \gg \left| \frac{F_{jxx} f^{-2}}{F_j} \int_0^{-h} z N^2(z) dz \right|$$

to be barotropic. Since, for large enough j ,

$$\begin{aligned} \left| \frac{F_{jxx} f^{-2}}{F_j} \int_0^{-h} z N^2(z) dz \right| \sim & \left| \frac{h_x}{h} \right| (j-1)^2 \pi^2 f^{-2} T_b^{-2} \\ & \times \int_0^{-h} z N^2(z) dz \{1 + O[(j-1)^{-1}]\}, \end{aligned}$$

the barotropic eigenfunctions eventually become baroclinic. Consequently the general result $c_j \sim j^{-1}$ for large enough j is not violated. Note, however, that since shelf motion is barotropic under (4.1), the baroclinic modes effectively do not make a significant contribution to the response and the large- j asymptotic analysis of the barotropic modes is therefore appropriate.

TABLE 1. Asymptotic results for the eigenfunctions, eigenvalues and various parameters in the barotropic case. Note that $F_j(x)$ is dimensionless and $O(1)$.

| | |
|----------------------------------|--|
| $F_j(x)$, large j | $(h_x h)^{-1/4} [(h_x h)^{1/4}]_{x=b} \sin\{(j-1)\pi T T_b^{-1}\} \{1 + O[(j-1)^{-1}]\}$ |
| c_j , large j | $(j-1)^{-2} \pi^{-2} f T_b^2 \{1 + O(j-1)^{-2}\}$ |
| D_j , large j | $\frac{1}{2} [(h h_x)^{1/2}]_{x=b} T_b \{1 + O[(j-1)^{-1}]\}$ |
| b_j , any j | $O[(j-1)^{-1}]$ |
| a_{jj} , large j | $-(j-1)^2 \pi^2 f^{-1} T_b^{-3} (\int_b^a r(h_x)^{1/2} (h^{-3/2}) dx) \{1 + O[(j-1)^{-1}]\}$ |
| a_{ij} , fixed i , large j | $O[(j-1)^{-1}]$ |
| a_{ij} , fixed j , large i | $O[(j-1)^{-1}]$ |
| $-[a_{ij} c_j]^{-1}$ | $T_b (\int_b^a r(h_x)^{1/2} h^{-3/2} dx)^{-1} \{1 + O[(j-1)^{-1}]\}$ |

From the results in Table 1 we have that the left-hand side of Eq. (3.2) is of order $[(j-1)^2] \phi_j$. The right-hand side is $O[(j-1)^{-1}]$ provided the infinite sum is convergent [verifiable a posteriori using Table 1 and (4.6a)]. Thus,

$$\phi_j = O(j-1)^{-3} \tag{4.6a}$$

$$p_j = F_j \phi_j = O\{(j-1)^{-3} \sin[T(j-1)\pi T_b^{-1}]\} \tag{4.6b}$$

$$v_j = \frac{p_{jx}}{f} = \frac{F_{jx}}{f} \phi_j = O\{(j-1)^{-2} \cos[T(j-1)\pi T_b^{-1}]\}. \tag{4.6c}$$

The preceding results indicate that fewer modes should be necessary to describe pressure (and hence coastal sea level) than alongshore currents. This has also been pointed out in less general circumstances by Hsieh (1982). It is straightforward to use (4.6) to verify that the infinite sum expressions for v and p are uniformly convergent. Since v is uniformly convergent, Eq. (2.19), which we needed earlier, is valid.

Finally, we note from Table 1 that the e -folding spinup time in the barotropic case for mode j is

$$(-a_{ij} c_j)^{-1} = \left(\int_b^a (h_x)^{1/2} h^{-1/2} dx \right) / \left(\int_b^a r(h_x)^{1/2} h^{-3/2} dx \right) \times \{1 + O[(j-1)^{-1}]\}. \tag{4.7}$$

Since this spinup time is independent of j (at lowest order) and (4.7) is correct in order of magnitude for even low mode numbers j (see the West Florida Shelf example in Table 3), the right-hand side of (4.7) is a good estimate of the model barotropic spinup time.

In the case that the shelf slope and r are independent of x , (4.7) can be simplified to

$$(-a_{ij} c_j)^{-1} = r^{-1} [h(a)h(b)]^{1/2} \{1 + O[(j-1)^{-1}]\}. \tag{4.8a}$$

Since $h(b) = 3\delta$ and $r = f\delta/2$, (4.8a) can also be written in the form

$$(-a_{ij} c_j)^{-1} = 2f^{-1} \left(\frac{3h(a)}{\delta} \right)^{1/2} \{1 + O[(j-1)^{-1}]\}. \tag{4.8b}$$

b. Convergence properties in the purely baroclinic case

For $|Nh_x f^{-1}| > 1$, Chapman and Hendershott (1982) showed that coastal trapped waves behave like internal Kelvin waves. Under the more restrictive condition $|Nh_x f^{-1}| \gg 1$ coastal-trapped waves do in fact reduce to coastal internal Kelvin waves with eigenfunctions of the form

$$F_j(x, z) = \exp[-f(x-b)c_j^{-1}] R_j(z). \tag{4.9}$$

The eigenfunctions $R_j(z)$ and eigenvalues c_j are found by solving the Sturm-Liouville system

$$\left(\frac{R_z}{N^2} \right)_z + \frac{R}{c^2} = 0, \tag{4.10a}$$

$$R_z = 0 \text{ on } z = 0, -H \tag{4.10b, c}$$

where H is the water depth in the constant-depth deep sea region. [That the Kelvin wave solution defined by (4.9) and (4.10) does solve the general eigenvalue problem (2.8) and (2.9) in the limit $|Nh_x f^{-1}| \gg 1$ can be verified by direct substitution. The field equation and all boundary conditions except the bottom boundary condition are satisfied exactly. The latter condition is satisfied with relative error $N^{-1} h_x^{-1} f \ll 1$ because (4.10a) shows that $R_z R^{-1} \sim N/c$.]

The solution defined above can be used to find the baroclinic asymptotic results. A WKB analysis in appendix B shows that

$$R_j(z) = \text{constant } N^{1/2} \cos \left[\frac{S_j \pi}{S_H} \right] (1 + O(j^{-1})) \tag{4.11}$$

$$c_j = -S_H j^{-1} \pi^{-1} [1 + O(j^{-4})] \tag{4.12}$$

$$c_j = -S_H j^{-1} \pi^{-1} [1 + O(j^{-4})] \quad (4.12)$$

where

$$S = S(z) = \int_0^z N dz, \quad (4.13a)$$

$$S_H = S(-H). \quad (4.13b)$$

In Table 2 the constant in (4.11) is chosen so that $F_j(b, 0) = 1$. These results and the other asymptotic results in Table 2 are discussed in appendix B.

In a similar fashion to the barotropic case, we can deduce, using Table 2 results and Eq. (3.2), that for large j

$$\phi_j \sim j^{-2} \sin(j\theta), \quad (4.14a)$$

$$p_j = F_j \phi_j \sim j^{-2} \sin(j\theta) \cos\left(\frac{S_j \pi}{S_H}\right) \left[\exp\left(\frac{\pi f(x-b)}{S_H}\right) \right]^j \quad (4.14b)$$

$$v_j = \frac{p_{jx}}{f} = f^{-1} F_{jx} \phi_j \sim j^{-1} \sin(j\theta) \cos\left(\frac{S_j \pi}{S_H}\right) \times \left[\exp\left(\frac{\pi f(x-b)}{S_H}\right) \right]^j. \quad (4.14c)$$

As in the barotropic case, the results indicate that pressure converges more rapidly than alongshore velocity implying that fewer modes should be necessary to describe coastal sea level than alongshore currents. By standard analysis it is very possible to verify that $v = p_x f^{-1}$ is uniformly convergent and therefore that (2.19) is valid. Note, however, that at $x = b$, the right-hand side of (2.18) is not convergent. This is the motivation for taking space in section 2 to explain how

(2.19) rather than (2.18) can be used in deriving the theoretical results.

A comparison of the barotropic and baroclinic results for p_j and v_j indicates that more terms are needed to obtain the p and v fields in the baroclinic case. At $x = b$, the convergence in the baroclinic case is, in fact, very slow because for *small* or even *moderate* j , $j\theta$ is small enough that

$$j^{-1} \sin(j\theta) = \theta. \quad (4.15)$$

By (4.14c) this means that the alongshore velocity v will not really be convergent until (4.16) begins to break down. For constant $N(z)$, θ , which is defined in Table 2, can be simplified to

$$\theta = \pi h(b) H^{-1} = \frac{1}{42.4} \quad (4.16)$$

for the representative values $h(b) = 30$ m, $H = 4$ km. Taking the number j of modes necessary for v to be convergent to be defined by $j\theta = \pi/2$, more than 67 modes are necessary in the case of constant N , $|N h_x f^{-1}| \gg 1$. More typically, for exponentially decaying N and reasonable parameter values, about 30 modes are necessary.

Along with the above very slow convergence, we should keep in mind that convergence seaward of $x = b$ is much faster. This is due to the factor

$$\{\exp[\pi f(x-b) S_H^{-1}]\}^j$$

in (4.14b) and (4.14c). For example, it takes only 3 modes for the p and v fields to converge within 10% at a distance $\frac{1}{2} |c_1/f|$ from $x = b$.

From Table 2 the spinup time $(-c_j a_{jj})^{-1}$ for mode j is, for the limit $j \rightarrow \infty$,

TABLE 2. Asymptotic results for the eigenfunctions, eigenvalues and various parameters in the purely baroclinic case. The parameters θ , N_0 and \bar{N} are defined by $\theta = \pi S(-h(b))/S_H$, $N_0 = N(0)$ and $\bar{N} =$ depth averaged $N(z) = H^{-1} \int_{-H}^0 N dz$. In estimating a_{jj} , a_{ij} and $-[a_{jj}c_j]^{-1}$ it was assumed, for simplicity, that $N(-h(b)) = N_0$ and $S(-h(b)) = -h(b)N_0$.

| | |
|----------------------------------|---|
| $F_j(x, z)$, large j | $N^{1/2} N_0^{-1/2} \exp[-f(x-b)/c_j] \cos(S_j \pi/S_H) [1 + O(j^{-1})]$ |
| c_j , large j | $-\frac{S_H}{j\pi} (1 + O(j^{-2})) = \frac{\bar{N}H}{j\pi} [1 + O(j^{-2})]$ |
| D_j , large j | $-\frac{1}{2} N_0^{-1} S(-h(b)) [1 + O(j^{-1})]$ |
| b_j , large j | $\frac{\sin(j\theta)}{j\theta} \{2N_0^{1/2} [N(-h(b))]^{-1/2} [h(b)]^{-1}\} [1 + O(j^{-1})]$ |
| a_{jj} , large j | $-c_j^{-1} \sin^2(j\theta) r(b)/h(b) [1 + O(j^{-1})] = -\frac{1}{6} c_j^{-1} \sin^2(j\theta) f [1 + O(j^{-1})]$ |
| a_{ij} , fixed i , large j | $-2f^{-1} \frac{\sin(j\theta)}{j\theta} \left\{ h_x^{-1} \frac{d}{dx} \left[r \frac{\partial F_i}{\partial x}(x, -h(x)) \right] - h^{-1} r \frac{\partial F_i}{\partial x}(x, -h(x)) \right\}_{x=b} [1 + O(j^{-1})]$ |
| a_{ij} , fixed j , large i | $c_i^{-1} \cos(i\theta) r(b) F_j(b, -h(b)) D_j^{-1} [1 + O(i^{-1})]$ |
| $-[a_{jj}c_j]^{-1}$ | $\left[h(b) + \frac{1}{2} c_j h_x(b) f^{-1} \right] / \left\{ r(b) \left[\sin^2(j\theta) + \frac{1}{2} j^{-1} \theta^{-1} \sin(2j\theta) \right] + \frac{1}{4} r_x(b) c_j f^{-1} \right\} [1 + O(j^{-1})]$ |

$$\frac{h(b)}{r(b) \sin^2(j\theta)} = 6f^{-1}(\sin j\theta)^{-2}$$

However, by the analysis in the previous paragraph, the response is dominated by the first 30 or so modes and for these modes the $O(j^{-1})$ terms in the formula for $(-c_j a_{jj})^{-1}$ in Table 2 cannot be neglected. Thus the spinup time for the modes that really matter is a complicated function of j . Using realistic parameter values and $Nh_x f^{-1} = 10$ gives modal spinup times between several days and a few months. This means that the model spinup time in the purely baroclinic case is much longer than in the barotropic case.

c. The intermediate case

Many wide continental shelves satisfy the condition $|Nh_x f^{-1}| \ll 1$ over the shelf and the theory of section 4a can be used. For almost all the remaining continental shelves, however, neither the limiting case of section 4a ($|Nh_x f^{-1}| \ll 1$ on the shelf) nor the limiting case of section 4b ($|Nh_x f^{-1}| \gg 1$ over the shelf and slope) is applicable. For example, for Australia's narrow southeastern continental margin in the Australian Coastal Experiment region $|Nh_x f^{-1}|$ averages 0.77 on the shelf and 2.3 on the continental slope. For these intermediate cases, the two-dimensional eigenfunctions $F_j(x, z)$ and eigenvalues c_j must be obtained numerically and asymptotic results for v_j and p_j are therefore not readily available.

Although we cannot establish convergence in general in the intermediate case, it is to be expected from physical grounds and the fact that convergence occurs in the two limiting cases. Given that convergence occurs, a problem still exists since it is not completely clear how many modes need to be included to approximate the solution adequately. Battisti and Hickey (1984) present calculations suggesting that mode 1 can quantitatively describe coastal sea level at coastal stations on the Oregon and Washington shelves (an intermediate case). However, consistent with our finding that more modes are necessary to describe currents than pressure, Battisti and Hickey found that currents were not so well described by the single first mode. In an inviscid intermediate case calculation for the Australian Coastal Experiment Region, Clarke and Thompson (1984) established convergence for non-nearshore pressure and alongshore velocity using the first five modes. Clarke and Thompson's method for establishing convergence cannot easily be applied in other cases, however.

One general way to test for convergence is to test how accurately the field equations and boundary conditions (2.1) and (2.2) are satisfied by the finite-sum approximation to the solution (2.13), viz.,

$$p = \sum_{j=1}^M F_j(x, z) \phi_j(y, t). \tag{4.17}$$

The properties of the $F_j(x, z)$ imply that the field equation and all boundary conditions except (2.2a) and (2.2c) are automatically satisfied by the finite solution. In terms of ϕ_j , the boundary conditions (2.2a) and (2.2c), using (4.17), (2.9b), (2.9c) and (3.2), can be written

$$\left[\sum_{j=1}^M F_j(b_j \tau^y - \sum_{i=1}^M a_{ij} \phi_i) - \frac{r}{h} \sum_{j=1}^M F_j \phi_j / c_j \right]_{x=b} - \frac{\tau^y}{h(b)} = \epsilon_M^{(1)} \tag{4.18}$$

$$\left\{ \sum_{j=1}^M h_x f F_j(b_j \tau^y - \sum_{i=1}^M a_{ij} \phi_i) + \sum_{j=1}^M [(r F_{jx})_x - h_x r F_{jxz}] \phi_j \right\}_{z=-h(x)} = \epsilon_M^{(2)}. \tag{4.19}$$

For appropriate convergence, we thus just need to take M large enough to reduce $|\epsilon_M^{(1)}|$ and $|\epsilon_M^{(2)}|$ to be smaller than the necessary error level.

5. An example

a. Background

A simple West Florida Shelf example will be used here to illustrate the model and indicate some of its properties. A comparison of the Clarke and Van Gorder model with actual West Florida Shelf observations using measured wind data as input is given by Mitchum and Clarke (1986b).

The West Florida Shelf (see Fig. 1) is very wide and shallow. Strongest wind driven currents occur in the wintertime. For this season N_s , the average buoyancy frequency on the shelf, is 10^{-3} s^{-1} . Using the representative values $\alpha_s = 5.75 \times 10^{-4}$ and $f = 6.6 \times 10^{-5}$ we have

$$\frac{N_s \alpha_s}{f} = 8.7 \times 10^{-3} \ll 1. \tag{5.1}$$

From (5.1) and the results of Clarke and Brink (1985), the eigenfunctions are independent of z and therefore satisfy (4.2) and (4.3).

The wind stress in the winter time consists largely of weather systems that propagate southward along the shelf. For simplicity, we model this by

$$\tau^y(y, t) = \tau_0^y \cos(ly + \omega t) \tag{5.2}$$

with $\omega/l = -10 \text{ m s}^{-1}$ and $\omega = 10^{-5} \text{ s}^{-1}$.

Mitchum and Clarke (1986b) found that current and sea level fluctuations on the West Florida Shelf were mainly driven by winds blowing over the West Florida Shelf, i.e., that the energy flux entering around the

Florida Keys was small. In our simple model, we will ignore the energy flux at the Florida Keys ($y = 0$) and consequently put

$$\phi_j(0, t) = 0 \quad \text{for all } j. \quad (5.3)$$

Note that our x -axis points outward from the coast along the Keys so if we define L to be the alongshore distance from the closed to open end of the "box," then the region of interest is $-L \leq y \leq 0, b \leq x \leq a$.

Although the model permits slow variation of parameters alongshore, for simplicity we took $a, b, h(a)$ and $h(b)$ to be constant. Appropriate values for $a - b, h(a), h(b)$ and L were found to be 100 km, 80 m, 22.5 m and 600 km. The value for $h(b)$ was based on $h(b) = 3\delta$ and the estimates of δ by Mitchum and Sturges (1982) and Marmorino (1983). Here $r = f\delta/2$, and the shelf bottom slope h_x were taken to be constant and equal to $2.48 \times 10^{-4} \text{ m s}^{-1}$ and 5.75×10^{-4} , respectively. Under the approximation that the shelf slope is constant, the eigenfunctions $F_j(x)$ have the Bessel Function form

$$F_j(x) = \text{constant} [J_0(\xi)Y_0(\xi_a) - Y_0(\xi)J_0(\xi_a)] \quad (5.4a)$$

where J_0 and Y_0 are zero-order Bessel Functions and

$$\xi = \xi(x) = 2(fxc_j^{-1})^{1/2}, \quad \xi_b = \xi(b), \quad \xi_a = \xi(a). \quad (5.4b)$$

Table 3 shows the parameter values $c_j, b_j, (-a_{jj}c_j)^{-1}$ and a_{ij} calculated using (5.4) and (A12)–(A15) of appendix A.

The ϕ_j were calculated using the method of section 3 and (5.2) with $\Delta t = 10.9$ hours and $\Delta y = 600$ m. We used 7 modes in the calculations. This gave (root mean

squared $\epsilon_M^{(1)}/(\text{root mean squared } \tau^y/h(b)) \approx 0.03$ to 0.04 [see (4.18)].

A number of sea level and velocity calculations were carried out and these are summarized by Figs. 2–11. In all of the figures 'phase' refers to the phase in degrees that the sea level or velocity field lags the wind stress at $y = 0$.

b. Results of the fully coupled calculation

As predicted by the asymptotics discussed in section 4, for the same accuracy, more modes were necessary to describe alongshore currents than sea level (7 compared with 4).

1) THE SEA LEVEL FIELD

The sea level amplitude field (see Fig. 2a) shows a monotonic increase northward and a monotonic decrease offshore. The phase (see Fig. 2b) decreases toward the north indicating northward phase propagation. Phase differences along $x = b$ are negligible. These properties are also found at realistic higher ($\omega = 1.6 \times 10^{-5} \text{ s}^{-1}$) and lower ($\omega = 4 \times 10^{-6} \text{ s}^{-1}$) frequencies.

The sea level field is dominated by the first mode (see Figs. 2a and 4). Mitchum and Clarke (1986b) found this result to be true for more realistic forcing and were able to interpret the sea level field as being largely due to the sum of a forced and free wave which cancel at the Keys.

Observe that sea level phase is everywhere approximately 180° out of phase with the wind stress at $y = 0$. To see why this should be so, consider the depth-integrated y -momentum equation in "deep" water $x \geq b$:

TABLE 3. The coefficients $c_j, b_j, (-a_{jj}c_j)^{-1}$ and a_{ij} for the West Florida Shelf model discussed in section 5 of the text for the first 7 modes. Asymptotic values using Table 1 results are shown in brackets. The a_{ij} are in units of m^{-1} when multiplied by 10^{-6} . The constant in (5.4a) is chosen so that D_j has the same value as in the asymptotic case, viz., $\frac{1}{2}[(hh_x)^{1/2}]_{x=b}T_b = 19.926 \text{ m}$.

| j | c_j (ms^{-1}) | b_j (m^{-1}) | $(-a_{jj}c_j)^{-1}$ (days) | a_{1j} | a_{2j} | a_{3j} | a_{4j} | a_{5j} | a_{6j} | a_{7j} |
|-----|-------------------------------|------------------------------|-------------------------------|---------------|---------------------|----------------------|----------------------|----------------------|----------------------|----------------------|
| 1 | 5.471 (∞) | .0357 | 2.18 (1.98) | -0.971 (0) | -1.007 | -0.349 | -0.375 | -0.175 | -0.225 | -0.116 |
| 2 | 0.621 (0.821) | .0219 | 1.83 (1.98) | -1.007 | -10.213 (-7.106) | -5.144 | -1.877 | -1.731 | -0.944 | -1.042 |
| 3 | 0.189 (0.205) | .0131 | 1.91 (1.98) | -0.349 | -5.144 | -31.968 (-28.424) | -12.486 | -4.099 | -3.569 | -1.900 |
| 4 | 0.088 (0.091) | .0091 | 1.94 (1.98) | -0.375 | -1.877 | -12.486 | -67.616 (-63.954) | -23.293 | -7.085 | -5.895 |
| 5 | 0.050 (0.051) | .0069 | 1.97 (1.98) | -0.175 | -1.731 | -4.099 | -23.293 | -117.40 (-113.70) | -37.650 | -10.879 |
| 6 | 0.032 (0.033) | .0056 | 1.97 (1.98) | -0.225 | -0.944 | -3.569 | -7.085 | -37.650 | -181.38 (-177.65) | -55.572 |
| 7 | 0.023 (0.023) | .0047 | 1.98 (1.98) | -0.116 | -1.042 | -1.900 (-0.492) | -5.895 | -10.879 | -55.572 | -259.56 (-255.82) |

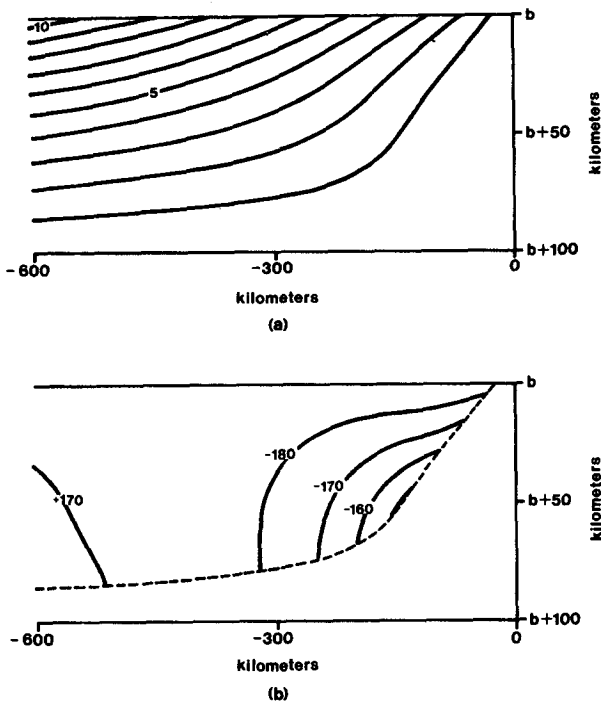


FIG. 2. (a) Amplitude (in cm) and (b) phase (in deg) of the sea level response to the idealized forcing given by Eq. (5.2) for the standard fully coupled case. For contour clarity the cross-shelf scale has been made one half of the alongshelf scale. Tick marks on the rectangle correspond to those in Fig. 1. The amplitude contour interval is 1 cm. Phase is not shown when the amplitude is less than 1 cm.

$$hv_t + hfu + hg\eta_y = \frac{\tau^y}{\rho_0} - rv. \quad (5.5)$$

At $x = b$ the transport hu perpendicular to the coast vanishes (Mitchum and Clarke, 1986a) giving an equation equivalent to (2.2a). At $y = 0$, v is also zero so at $x = b$, $y = 0$ we have the balance

$$g\eta_y = \frac{\tau^y}{\rho_0 h(b)}. \quad (5.6)$$

For distances y small compared to the scale of the wind we may thus write

$$\eta \approx \frac{y(\tau^y)_{y=0}}{\rho_0 g h(b)}. \quad (5.7)$$

Solutions of this form for a semi-infinite shelf have been obtained previously by Clarke and Thompson (1984) and Mitchum and Clarke (1986a). Since $y < 0$ and the alongshore scale of the wind stress is larger than the length L of the shelf, we expect the $x = b$ sea level to be approximately 180° out of phase with the wind stress and to increase in amplitude to the north. Seaward of $x = b$ this result still holds because the response is dominated by mode 1 which has no zeros cross-shelf.

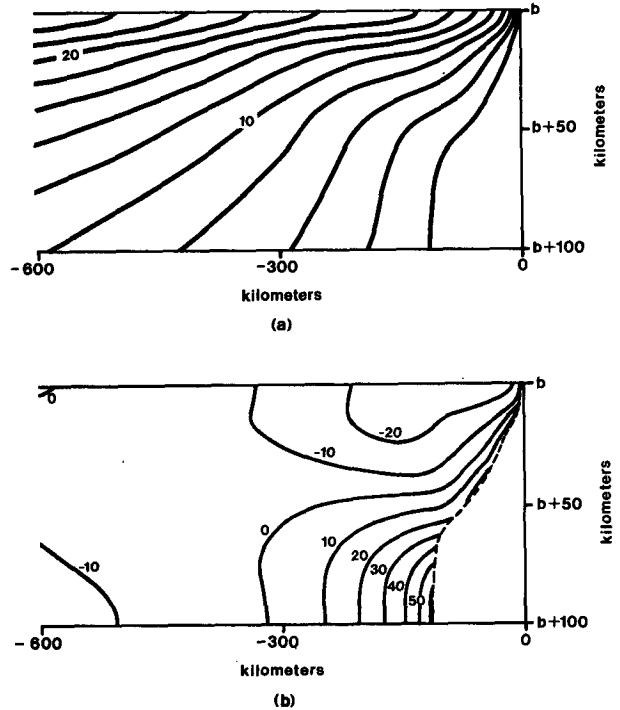


FIG. 3. Alongshore velocity (a) amplitude (in cm s^{-1}) and (b) phase (in deg) for the standard fully coupled case. Tick marks and rectangle scales are as described in Fig. 2. The amplitude contour interval is 2 cm s^{-1} . Phase is not shown when the amplitude is less than 2 cm s^{-1} .

2) THE ALONGSHORE VELOCITY FIELD

The alongshore-velocity amplitude field (see Fig. 3a) shows a monotonic decrease in amplitude offshore and a monotonic increase northward. Most of the variance of the current is shoreward of the 50-m isobath which is roughly halfway between $x = b$ and $x = b + 100 \text{ km}$. The alongshore-velocity phase field indicates variable propagation behavior. Nearshore propagation is southward and offshore propagation is northward. In contrast to the sea level field, the velocity field is not dominated by the first mode, especially nearshore (compare Figs. 3a and 3b with Fig. 5).

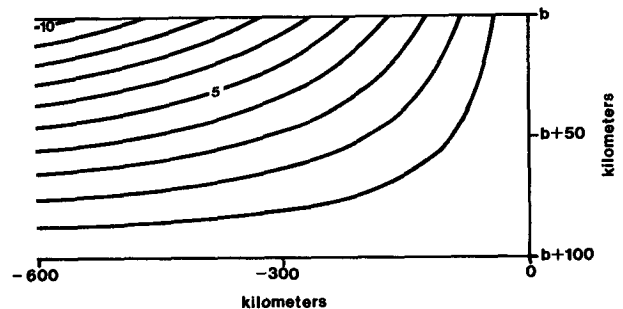


FIG. 4. Sea level amplitude response as in Fig. 2a except that only the first mode was used in the calculation. Phase is not shown since it was everywhere within nine degrees of 180° .

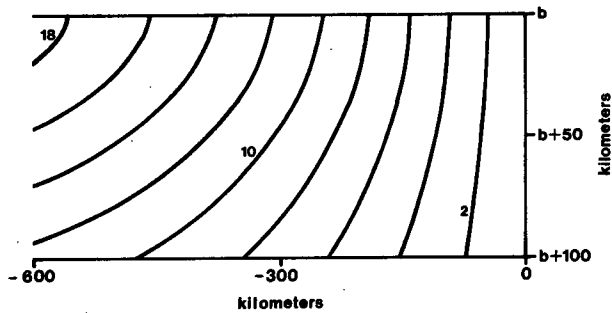


FIG. 5. Alongshore-velocity amplitude response as in Fig. 3a except that only one mode was used in the calculation. The alongshore velocity phase is not shown since it is everywhere within nine degrees of zero. The contour interval is 2 cm s^{-1} .

Note that although the velocity field phase is variable, over most of the region the velocity is nearly in phase with the wind stress. This in-phase relationship and the amplitude increase to the north are consistent with geostrophic balance, $p = 0$ at the shelf edge and the above discussion about sea level.

c. The decoupled case

How important is the scattering caused by friction? To test this, we carried out the calculations for exactly the same basic parameters as in section 5b but with decoupled equations, i.e., we put

$$a_{ij} = 0, \quad i \neq j. \quad (5.8)$$

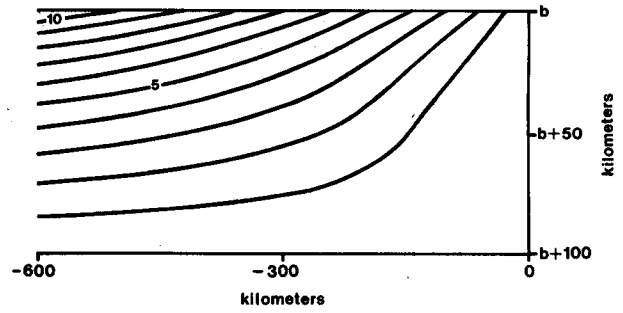
The sea level field (see Fig. 6) and the alongshore velocity field (see Fig. 7) are very similar qualitatively to the coupled case (see Figs. 2 and 3). The major quantitative difference occurs in the results for alongshore velocity amplitude which can be as much as 28% too high.

d. The Arrested-Topographic Wave and inviscid cases

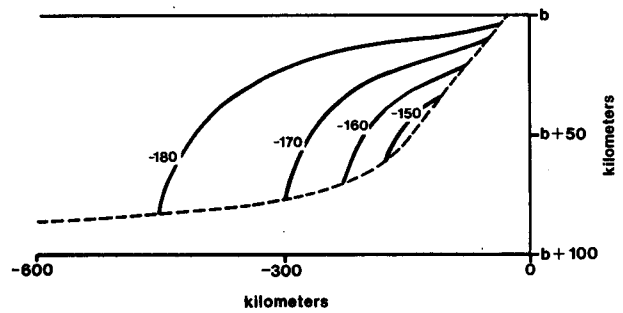
Arrested-Topographic Wave theory (Csanady, 1978) and Gill and Schumann's (1974) forced continental shelf wave theory are limiting cases of the theory described in section 2. Arrested-Topographic Wave theory applies when the motion is barotropic and $\partial/\partial t = 0$; Gill and Schumann's theory applies when the motion is barotropic and $r = 0$. As mentioned in the introduction, scaling shows that for "weather" frequency-band forcing and realistic friction, both limiting theories should be subject to significant error. We now demonstrate this using West Florida shelf model parameters.

1) THE ARRESTED-TOPOGRAPHIC WAVE CASE

We ran our West Florida Shelf model with exactly the same parameters as before except that we put $\omega = 10^{-10} \text{ s}^{-1}$. To within negligible error, this is equivalent



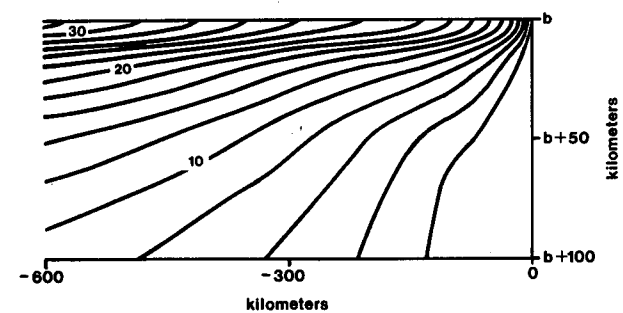
(a)



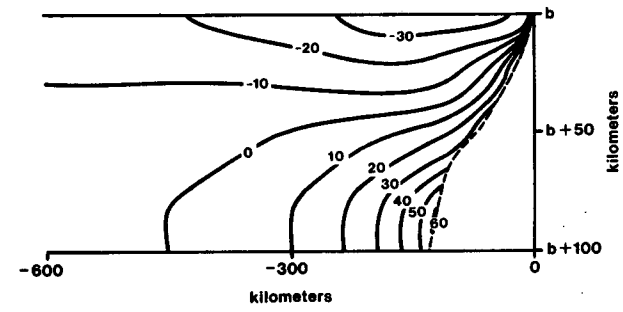
(b)

FIG. 6. Sea level response as in Fig. 2 except that $a_{ij} = 0, i \neq j$ (uncoupled forced wave equations case).

to putting $\partial/\partial t = 0$. Such a model is, strictly speaking, a modified version of Csanady's model because of the use of a different coastal boundary condition in each case. Csanady used



(a)



(b)

FIG. 7. Alongshore velocity response as in Fig. 3 except $a_{ij} = 0, i \neq j$ (uncoupled forced wave equations case).

$$\rho_0 r v = \tau^y \text{ at } x = 0 \quad (5.9)$$

while $\partial/\partial t = 0$ in (2.2a) and $v = p_x \rho_0^{-1} f^{-1}$ gives

$$\rho_0 r v + p_y h = \tau^y \text{ at } x = b. \quad (5.10)$$

Observe that Csanady's boundary condition cannot be satisfied at the Florida Keys where $v = 0, \tau^y \neq 0$.

The sea level and alongshore velocity field results for the Arrested-Topographic Wave calculations are shown in Figs. 8 and 9 respectively. While the plots are quite similar to the general case (Figs. 2 and 3), there are qualitative and quantitative errors in the Arrested-Topographic Wave solution. As expected, these errors increase as the frequency is increased.

2) THE INVISCID WAVE RESULTS

In this case we ran our model with $r = 0$. This is analogous to the Gill and Schumann case except that they obtained their solution in terms of a stream function and applied a different boundary condition at the seaward edge of their model.

The inviscid results are shown in Figs. 10 and 11. They differ markedly from the general case (Figs. 2 and 3). Large errors thus result if friction is omitted. The many short-scale features present are probably due to higher modes which are not damped.

6. Concluding remarks

Given measured wind stress forcing, stratification and shelf and slope topography, it is possible, using the

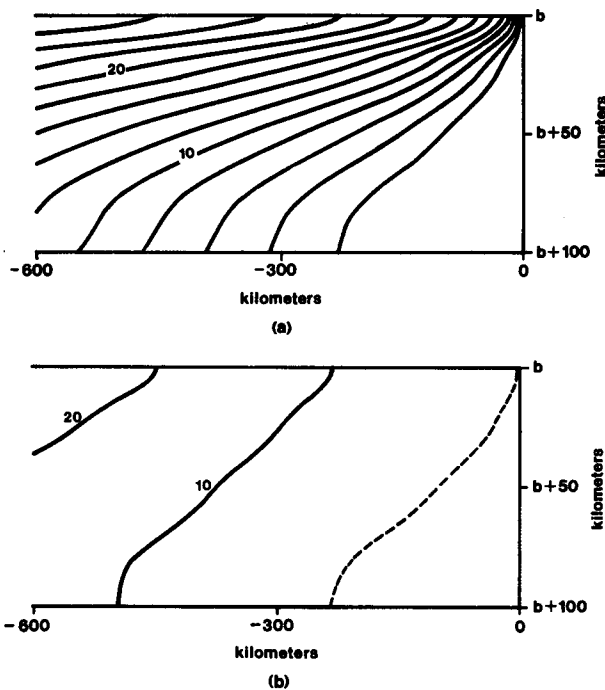


FIG. 9. Alongshore-velocity response as in Fig. 3 except that $\partial/\partial t = 0$ (Arrested-Topographic Wave case).

theory presented, to estimate wind-driven low-frequency current and sea level fluctuations on continental shelves. The theoretical structure allows for fairly straightforward computation and provides the means

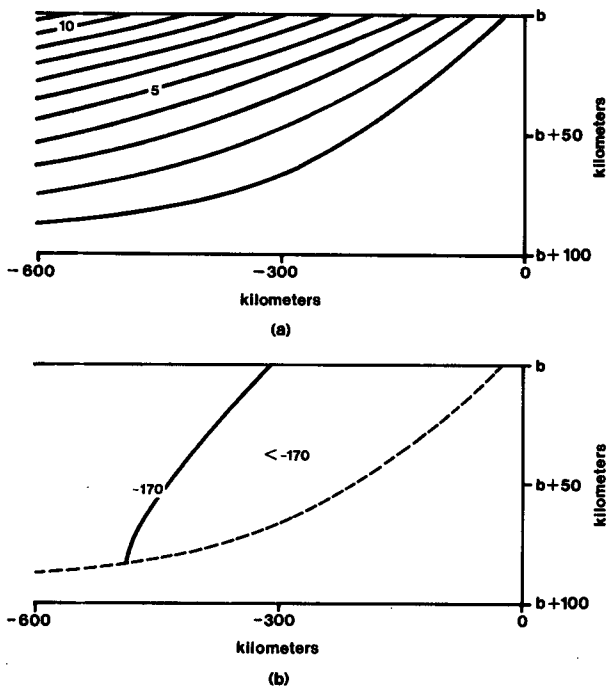


FIG. 8. Sea-level response as in Fig. 2 except that $\partial/\partial t = 0$ (Arrested-Topographic Wave case). The phase contour interval is 10° .

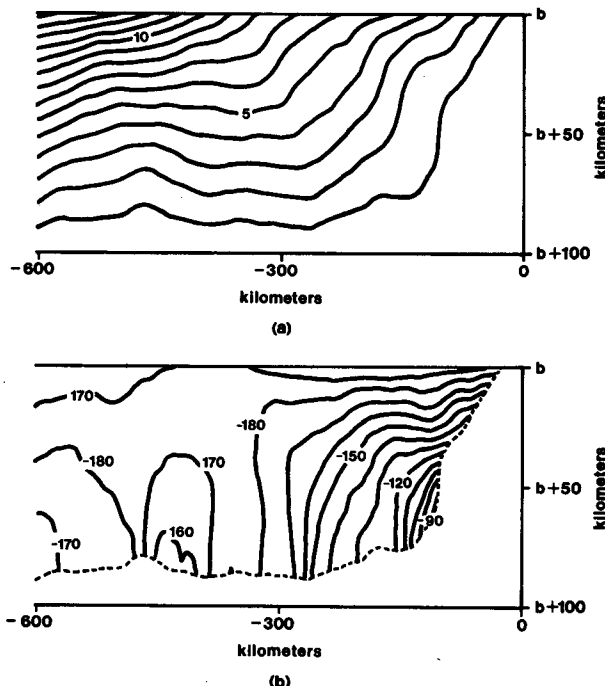


FIG. 10. Sea level response as in Fig. 2 except that $r = 0 \equiv a_{ij}$ (frictionless case).

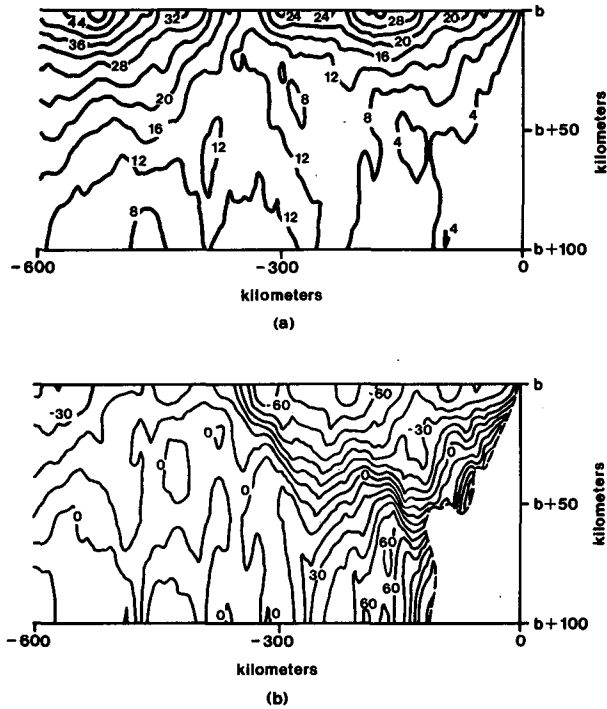


FIG. 11. Alongshore velocity response as in Fig. 3 except $r = 0 \equiv a_{ij}$ (frictionless case). The contour interval is 4 cm s^{-1} for the amplitude and 30° for the phase. Phase is not shown when the amplitude is less than 4 cm s^{-1} .

of quickly identifying the relevant physics in terms of coastal-trapped wave modes. Previous work (Clarke, 1977; Battisti and Hickey, 1984) using just one mode and an inaccurate measure of friction gave encouraging results. More recent tests using the more complete theory here on larger datasets from the Australian Coastal Experiment (Church et al., 1986) and the West Florida Shelf (Mitchum and Clarke, 1986b) suggest that the method is of practical use.

Acknowledgments. This work was supported by the National Science Foundation (Grants OCE-8300029 and OCE-8500669) and the Commonwealth Scientific and Industrial Research Organization, Australia. We are also grateful for helpful discussions with Dr. Ken Brink on his version of (2.16) and ours. The computations discussed in the footnote were mainly done by him. Paula Tamaddoni-Jahromi expertly typed the manuscript and drafted the figures.

This paper is dedicated to the memory of Dr. Adrian E. Gill.

APPENDIX A

Barotropic Results

1. Long shelf wave modes for general $h(x)$ and large mode number j

We wish to solve the longshelf-wave eigenvalue problem (4.2) and (4.3) for general $h(x)$ and large mode

number j . As mode number j increases, the x -scale of the solution decreases so that the topographic scale $(h_x/h)^{-1}$ is effectively a slowly varying function. This suggests that for large j a solution with slowly varying amplitude and rapidly varying phase, viz., a WKB type solution, should be valid.

Substitution of the WKB form

$$F(x) = B(x) \sin Q(x) \quad (\text{A1})$$

into (4.2) gives

$$\begin{aligned} B_{xx} \sin Q + 2B_x Q_x \cos Q - B(Q_x)^2 \sin Q \\ + BQ_{xx} \cos Q + \frac{h_x}{h} (B_x \sin Q + BQ_x \cos Q) \\ + \frac{h_x}{h} \mu B \sin Q = 0. \quad (\text{A2}) \end{aligned}$$

Following normal WKB practice that $B(Q_x)^2 \sin Q$ is a zero-order quantity, $BQ_{xx} \cos Q$, $2B_x Q_x \cos Q$ and $(h_x/h)BQ_x \cos Q$ are first order, $B_{xx} \sin Q$, $(h_x/h)B_x \sin Q$ are second order and μ is at an order to be determined, (A2) reduces, at zero order, to

$$(Q_x)^2 = \frac{\mu h_x}{h}. \quad (\text{A3})$$

Since $(h_x/h)\mu > 0$ for long continental shelf waves, Q_x is real. Without loss of generality, we take the positive square root and obtain

$$Q(x) = \int_a^x \left(\frac{h_x}{h} \mu \right)^{1/2} dx + \nu \quad (\text{A4})$$

for some arbitrary constant of integration ν .

At first order (A2) reduces to

$$2B_x Q_x + BQ_{xx} + BQ_x \frac{h_x}{h} = 0. \quad (\text{A5})$$

Using (A4), (A5) can be reduced to

$$\frac{B_x}{B} = -\frac{1}{4} \left(\frac{h_x}{h} \right)^{-1} \left(\frac{h_x}{h} \right)_x - \frac{1}{2} \left(\frac{h_x}{h} \right)$$

which can be integrated to give

$$B(x) = \text{constant} (h_x h)^{-1/4}. \quad (\text{A6})$$

Thus $F(x)$ is of the form (A1) with Q and B given by (A4) and (A6) respectively.

Satisfaction of the boundary condition at $x = a$ [see Eq. (4.3b)] implies that

$$\nu = m\pi \quad (\text{A7})$$

where m is an integer. The boundary condition at $x = b$, at lowest order, is

$$\mu B \sin Q = 0 \quad \text{at} \quad x = b. \quad (\text{A8})$$

Using the notation (4.5b) of the text, (A8) has eigensolutions μ_j of the form

$$\mu_j^{1/2} T_b = (j + \text{integer})\pi \tag{A9}$$

for some fixed integer. In the case when the shelf has constant slope the exact eigenfunctions are Bessel functions [see Eqs. (5.4a, b)] and large j asymptotics show that the fixed integer in (A9) is -1 . Thus at lowest order

$$\mu_j^{1/2} T_b = (j - 1)\pi \tag{A10}$$

and consequently

$$F_j(x) = (h_x h)^{-1/4} [h_x h]_{x=b}^{1/4} \sin[(j - 1)\pi T T_b^{-1}] \times \{1 + O[(j - 1)^{-1}]\}. \tag{A11}$$

Note that the constant in (A6) has been chosen so that $F_j(x)$ is dimensionless and $O(1)$. We also point out that (A11) is a lowest (zeroth) order solution even though $B(x)$ was determined from the first order field equation. The $O[(j - 1)^{-1}]$ first order solution follows a similar pattern, being determined by the second order field equation and first order boundary conditions.

2. Evaluation of the coefficients D_j , b_j , a_{jj} and a_{ij}

Since the motion is barotropic the general formulae (2.15)–(2.17) simplify to

$$D_j = h(b)[F_j(b)]^2 + \int_b^a (F_j(x))^2 h_x dx \tag{A12}$$

$$b_j = D_j^{-1} F_j(b) \tag{A13}$$

$$a_{ij} = \left[\int_b^a F_j \frac{d}{dx} (r F_{ix}) dx + [r F_j F_{ix}]_{x=b} \right] f^{-1} D_j^{-1} \tag{A14a}$$

$$= \left(- \int_b^a r F_{ix} F_{jx} dx \right) f^{-1} D_j^{-1}. \tag{A14b}$$

Evaluation of (A12)–(A14) using $F_j(x)$ given in (A11) is straightforward, provided one integrates appropriately by parts. As an example, the formula for a_{ij} is derived as follows.

Using Eqs. (A11) and (A14b) we have

$$-f D_j a_{ij} = \int_b^a r \left[(h_x h)^{-1/4} [(h_x h)^{1/4}]_{x=b} (j - 1) \times \pi T_x T_b^{-1} \cos[(j - 1)\pi T T_b^{-1}] \right]^2 \times dx \{1 + O[(j - 1)^{-1}]\}. \tag{A15}$$

Substituting for D_j and T_x from Table 1 and (4.5a) and then simplifying gives

$$a_{ij} = -(j - 1)^2 \pi^2 T_b^{-3} f^{-1} \int_b^a r (h_x)^{1/2} h^{-3/2}$$

$$\times \left[1 + \cos[2(j - 1)\pi T T_b^{-1}] \right] dx \{1 + O[(j - 1)^{-1}]\}. \tag{A16}$$

Since

$$\frac{d}{dx} \sin(2(j - 1)\pi T T_b^{-1}) = -2h_x^{1/2} h^{-1/2} (j - 1)\pi T_b^{-1} \cos[2(j - 1)\pi T T_b^{-1}],$$

the right-hand side of (A16) can be integrated by parts to show

$$a_{ij} = -(j - 1)^2 \pi^2 T_b^{-3} f^{-1} \int_b^a r (h_x)^{1/2} h^{-3/2} \times dx \{1 + O[(j - 1)^{-1}]\} \tag{A17}$$

which is the result shown in Table 1.

APPENDIX B

Baroclinic Results

1. $R_j(z)$ and c_j for large j

To deduce the baroclinic results, it is necessary to obtain the eigenvalues and eigenfunctions of the Sturm-Liouville problem (4.10) for large mode number j . We do this by an analogous WKB procedure to that in appendix A and find that at lowest order

$$R_j(z) = (\text{constant}) N^{1/2} \times \cos \left[\frac{S_j \pi}{S_H} \right] [1 + O(j^{-1})] \tag{B1}$$

$$c_j = -S_H j^{-1} \pi^{-1} [1 + O(j^{-2})]. \tag{B2}$$

Solutions of the eigenvalue problem (4.10) are widely used so we point out that for realistic stratification the asymptotic approximations (B1) and (B2) can be quite accurate for surprisingly small j . Numerical solutions of $R_j(z)$ and c_j for stratification in the Australian Coastal Experiment region (see Fig. 2 of Clarke and Thompson, 1984) were within 5% of the asymptotic estimates for $j \geq 4$. For the $j = 1$ case the error was 5% for c_j and 36% for R_j and the numerical and asymptotic estimates for the eigenfunctions were qualitatively very similar. [The error in R_j was calculated as

$$\left\{ \sum_{k=1}^K [R_j(z_k) - R'_j(z_k)]^2 / \sum_{k=1}^K [R_j(z_k)]^2 \right\}^{1/2}$$

where $R_j(z_k)$ represents the numerical solution at grid point $z = z_k$, $R'_j(z_k)$ the asymptotic estimate at that gridpoint and K the total number of grid points.]

2. Evaluation of the coefficients D_j , b_j , a_{jj} and a_{ij}

The coefficients can be evaluated by standard integration using appropriate integration by parts as illustrated in appendix A. The results are shown in Table 2.

REFERENCES

- Battisti, D. S., and B. M. Hickey, 1984: Application of remote wind-forced coastal trapped wave theory to the Oregon and Washington coasts. *J. Phys. Oceanogr.*, **14**, 887-903.
- Brink, K. H., 1982: The effect of bottom friction on low-frequency coastal trapped waves. *J. Phys. Oceanogr.*, **12**, 127-133.
- , and J. S. Allen, 1978: On the effect of bottom friction on barotropic motion over the continental shelf. *J. Phys. Oceanogr.*, **8**, 919-922.
- Chapman, D. C., and M. C. Hendershott, 1982: Shelf wave dispersion in a geophysical ocean. *Dyn. Atmos. Oceans*, **7**, 17-31.
- Church, J. A., N. J. White, A. J. Clarke, H. J. Freeland and R. L. Smith, 1986: Coastal trapped waves on the East Australian Continental Shelf. Part II: Model verification. Submitted to *J. Phys. Oceanogr.*
- Clarke, A. J., 1976: Coastal upwelling and coastally trapped long waves. Ph.D. thesis, Cambridge University, 178 pp.
- , 1977: Observational and numerical evidence for wind-forced coastal trapped long waves. *J. Phys. Oceanogr.*, **7**, 231-247.
- , and R. O. R. Y. Thompson, 1984: Large-scale wind-driven ocean response in the Australian Coastal Experiment Region. *J. Phys. Oceanogr.*, **14**, 338-352.
- , and K. H. Brink, 1985: The response of stratified, frictional shelf and slope waters to fluctuating large-scale low-frequency wind forcing. *J. Phys. Oceanogr.*, **15**, 439-453.
- Csanady, G. T., 1978: The arrested topographic wave. *J. Phys. Oceanogr.*, **8**, 47-62.
- Gill, A. E., and A. J. Clarke, 1974: Wind-induced upwelling, coastal currents and sea level changes. *Deep Sea Res.*, **21**, 325-345.
- , and E. H. Schumann, 1974: The generation of long shelf waves by the wind. *J. Phys. Oceanogr.*, **4**, 83-90.
- Hsieh, W. W., 1982: On the detection of continental shelf waves. *J. Phys. Oceanogr.*, **12**, 414-427.
- Marmorino, G. O., 1983: Variability of current, temperature, and bottom pressure across the West Florida Continental Shelf, Winter, 1981-1982. *J. Geophys. Res.*, **88**, 4439-4457.
- Mitchum, G. T., and W. Sturges, 1982: Wind-driven currents on the West Florida Shelf. *J. Phys. Oceanogr.*, **12**, 1310-1317.
- , and A. J. Clarke, 1986a: The frictional nearshore response to forcing by synoptic scale winds. *J. Phys. Oceanogr.*, **16**, 934-946.
- , and A. J. Clarke, 1986b: Evaluation of frictional, wind-forced long-wave theory on the West Florida Shelf. *J. Phys. Oceanogr.*, **16**, 1027-1035.
- Wang, D.-P., and C. N. K. Mooers, 1976: Coastal-trapped waves in a continuously stratified ocean. *J. Phys. Oceanogr.*, **6**, 853-863.